Strange and nonstrange quark mass dependence of elastic light resonances from SU(3) unitarized chiral perturbation theory to one loop

J. Nebreda and J. R. Peláez

Departamento de Física Teórica II, Universidad Complutense, 28040 Madrid, Spain

(Received 28 January 2010; published 31 March 2010)

We study the light quark mass dependence of the $f_0(600)$, $\kappa(800)$, $\rho(770)$, and $K^*(892)$ resonance parameters generated from elastic meson-meson scattering using unitarized one-loop chiral perturbation theory. First, we show that it is possible to fit simultaneously all experimental scattering data up to 0.8–1 GeV together with lattice results on decay constants and scattering lengths up to a pion mass of 400 MeV, using chiral parameters compatible with existing determinations. Then, the strange and nonstrange quark masses are varied from the chiral limit up to values of interest for lattice studies. In these amplitudes, the mass and width of the $\rho(770)$ and $K^*(892)$ present a similar and smooth quark mass dependence. In contrast, both scalars present a similar nonanalyticity at high quark masses. Nevertheless, the $f_0(600)$ dependence on the nonstrange quark mass is stronger than for the $\kappa(800)$ and the vectors. We also confirm the lattice assumption of quark mass independence of the vector two-meson coupling that, in contrast, is violated for scalars. As a consequence, vector widths are very well approximated by the Kawarabayashi-Suzuki-Riazuddin-Fayyazuddin relation, and their masses are shown to scale like their corresponding meson decay constants.

DOI: 10.1103/PhysRevD.81.054035 PACS numbers: 14.40.−n, 12.39.Fe, 13.75.Lb

I. INTRODUCTION

Although QCD is well established as the theory of strong interactions, the fact that its coupling becomes large at energies below 1–2 GeV keeps the hadronic realm beyond the reach of perturbative calculations. In that regime, lattice methods are a useful tool to calculate QCD observables, although the discretization involved in this technique introduces complications of its own, in particular, related to chiral symmetry breaking and the implementation of realistic small masses for the light quarks. Despite the remarkable success of lattice studies, results on light meson resonances are few and usually obtained at very large quark masses compared with their physical values [1,2]. This is particularly so for the light scalars, very relevant for nuclear attraction, but whose calculations are hindered by the so-called ''disconnected diagrams.'' Very recently [3], an alternative technique, based on chiral perturbation theory (ChPT) and dispersion relations, has been applied to calculate the dependence of the $f_0(600)$ (or ''sigma'') and $\rho(770)$ resonances on the pion mass—in practice, the average mass of the u and d quarks. Now the starting parameters are physical and resonances appear in amplitudes that describe real data on $\pi\pi$ scattering. The predicted dependence for the $\rho(770)$ compares remarkably well with previous and later lattice predictions. For the scalar sigma it shows a nonanalyticity that should be taken into account when extrapolating future lattice data to physical values. In this work we extend this study to include the strange quark mass within an SU(3) ChPT formalism. Our aim is threefold: first, to confirm previous results within a more general formalism. Second, to analyze the dependence on the average mass of the u and d quarks of the $K^*(892)$ and $\kappa(800)$ strange resonances. The latter, despite being a scalar, and very similar to the $f_0(600)$, is much more feasible for lattice calculations within the next few years [4] due to its nonzero isospin and strangeness. Third, we also study the dependence of all the $f_0(600)$, $\kappa(800)$, $\rho(770)$, and $K^*(892)$ parameters in terms of the strange quark mass. Finally, let us remark that the dependence of hadronic observables, meson masses in particular, is not only of relevance for lattice calculations, but also for anthropic considerations [5] or the study of the cosmological variability of fundamental constants [6].

Thus, in the next two sections we introduce very briefly the basic notation of ChPT, explain the relation between pseudoscalar meson and quark masses, and review the unitarization procedure. In Sec. II, we show the fits to the existing experimental data on elastic scattering as well as to lattice results on pion and kaon masses, their decay constants, and scattering lengths on the highest isospin channels. Section III is devoted to the dependence of light resonance properties on the nonstrange quark masses. In Sec. IV we then study the dependence with the strange quark mass and in Sec. V we present our summary and conclusions.

A. Chiral perturbation theory

As is well known, pions, kaons, and etas can be identified with the Nambu-Goldstone bosons (NGB) of the spontaneous chiral symmetry breaking of QCD. If quarks were massless, so should be the NGB and they would be separated by a mass gap of the order of 1 GeV from other hadrons, thus becoming the only relevant QCD degrees of freedom at low energies. Of course, quarks are not mass-

less, but the u, d, and s flavors have a sufficiently light mass to be considered as a perturbation. It is thus possible to write a low energy effective Lagrangian out of pion, kaon, and eta fields, known as chiral perturbation theory [7]. This Lagrangian is built as the most general derivative and mass expansion that respects the symmetries of QCD, particularly its chiral symmetry breaking pattern. Except for the leading order (LO), fixed by symmetry and the scale of spontaneous symmetry breaking, all terms in the Lagrangian are multiplied by a low energy constant (LEC) that contains the information on the underlying QCD dynamics and also renormalizes the loop diagrams with vertices from lower orders. In this way, pion, kaon, and eta observables are obtained as a *model independent* expansion in powers of momenta and masses over the chiral scale $4\pi f_0 \simeq 1.2$ GeV, where f_0 is the pion decay constant in the chiral limit (as it is customary, for quantities at leading order in the quark mass expansion we will use the 0 subscript).

In particular, partial wave amplitudes for elastic meson-meson scattering are obtained within ChPT as an expansion

$$t(s) = t_2(s) + t_4(s) + \cdots, \qquad t_{2k} = O(p^{2k}), \tag{1}$$

where p denotes either momenta or meson masses. Actually, these partial waves carry definite isospin I and total angular momentum J, but we have momentarily suppressed these labels for clarity. As we have just commented, the leading order $t_2(s)$ corresponds to the current algebra results and only depends on the scale of spontaneous chiral symmetry breaking f_0. The next-to-leading order $t_4(s)$ contains one-loop diagrams made of vertices from the lowest order Lagrangian, plus tree level diagrams of $O(p^4)$. Within the SU(3) formalism, these tree level diagrams are multiplied by LECs, denoted as L_i, which are independent of masses or momenta, and have been determined from different experiments. In Table I we provide several sets for the eight L_i that appear in meson-meson scattering to one loop. Those with an r superscript carry a dependence on the regularization scale μ [7], customarily chosen at $\mu = M_\rho$. Of course, that scale dependence cancels in the calculation of physical observables. The values in the second column come from the ''main fit'' of a K_{l4} analysis to two loops [8], whereas those in the third column come from the same reference, but to one loop. Naively one would expect the LECs obtained in our unitarized one-loop fits to lie somewhere in between these two sets of values, since unitarization reproduces one of the most relevant numerical contributions from the two-loop calculation, namely, the s-channel leading logs. As one of our main interests is πK scattering and the $K^*(892)$ and $\kappa(800)$ resonances, we also provide the values obtained from a very rigorous treatment of $K\pi$ scattering lengths in terms of the Roy-Steiner dispersion relations [9]. The rest of the columns correspond to unitarized ChPT fits that we will explain in Sec. II.

In this work, we are interested in the quark mass dependence of the amplitudes, which appears in ChPT through Lagrangian terms that contain the quark mass matrix $\mathcal{M} = \mathrm{diag}(\hat{m}, \hat{m}, m_s)$, that is treated as a perturbation. Note that we work in the isospin limit $\hat{m} \sim m_u = m_d = (m_u^{\mathrm{phys}} + m_d^{\mathrm{phys}})/2$. Chiral symmetry is explicitly broken by these mass terms and the NGB acquire masses, which, at leading order, read [7]

$$M_{0\pi}^2 = 2\hat{m}B_0, \qquad M_{0K}^2 = (\hat{m} + m_s)B_0, \qquad M_{0\eta}^2 = \frac{2}{3}(\hat{m} + 2m_s)B_0. \tag{2}$$

Let us recall that the constant B_0 is defined from the values *in the chiral limit* of the chiral condensate and the pion decay constant as follows: $B_0 = -\langle 0|\bar{q}q|0\rangle_0/f_0^2$, and thus it carries no quark mass dependence. To one loop, there are some corrections, and the physical meson masses now read

TABLE I. $O(p^4)$ chiral parameters ($\times 10^3$) evaluated at $\mu = M_\rho$. The second and third columns come from the two- and one-loop analysis listed in [8], where L_4 and L_6 were set equal to zero. The fourth column comes from a careful πK dispersive analysis [9] using the Roy-Steiner formalism. The IAM III column is one of the sets obtained from an older fit with the coupled channel IAM [10] (only statistical uncertainties are shown). The columns labeled Fit I and Fit II correspond to the simultaneous fit to experiment and lattice data performed in this work, which are described in Sec. II together with their uncertainties.

LECs	Ref. [8] $O(p^6)$	Ref. [8] $O(p^4)$	Ref. [9]	IAM III	Fit I	Fit II
L_1^r	0.53 ± 0.25	0.46	1.05 ± 0.12	0.6 ± 0.09	1.10	0.74
L_2^r	0.71 ± 0.27	1.49	1.32 ± 0.03	1.22 ± 0.08	1.11	1.04
L_3	-2.72 ± 1.12	-3.18	-4.53 ± 0.14	-3.02 ± 0.06	-4.03	-3.12
L_4^r	0 (fixed)	0 (fixed)	0.53 ± 0.39	0 (fixed)	-0.06	0.00
L_5^r	0.91 ± 0.15	1.46	3.19 ± 2.40	1.9 ± 0.03	1.34	1.26
L_6^r	0 (fixed)	0 (fixed)	$\cdots$	-0.07 ± 0.20	0.15	-0.01
L_7	-0.32 ± 0.15	-0.49	$\cdots$	-0.25 ± 0.18	-0.43	-0.49
L_8^r	0.62 ± 0.20	1.00	$\cdots$	0.84 ± 0.23	0.94	1.06
$L_8^r + L_6^r$	0.62 ± 0.20	1.00	3.66 ± 1.52	0.7 ± 0.46	1.24	1.04
$2L_1^r - L_2^r$	0.35 ± 0.57	-0.57	0.78 ± 0.24	-0.02 ± 0.20	1.09	0.44

$$M_\pi^2 = M_{0\pi}^2\Big[1 + \mu_\pi - \frac{\mu_\eta}{3} + \frac{16M_{0K}^2}{f_0^2}(2L_6^r - L_4^r) + \frac{8M_{0\pi}^2}{f_0^2}(2L_6^r + 2L_8^r - L_4^r - L_5^r)\Big], \tag{3}$$

$$M_K^2 = M_{0K}^2\Big[1 + \frac{2\mu_\eta}{3} + \frac{8M_{0\pi}^2}{f_0^2}(2L_6^r - L_4^r) + \frac{8M_{0K}^2}{f_0^2}(4L_6^r + 2L_8^r - 2L_4^r - L_5^r)\Big], \tag{4}$$

$$M_\eta^2 = M_{0\eta}^2\Big[1 + 2\mu_K - \frac{4}{3}\mu_\eta + \frac{8M_{0\eta}^2}{f_0^2}(2L_8^r - L_5^r) + \frac{8}{f_0^2}(2M_{0K}^2 + M_{0\pi}^2)(2L_6^r - L_4^r)\Big] + M_{0\pi}^2\Big[-\mu_\pi + \frac{2}{3}\mu_K + \frac{1}{3}\mu_\eta\Big] + \frac{128}{9f_0^2}(M_{0K}^2 - M_{0\pi}^2)^2(3L_7 + L_8^r),$$

$$\mu_P = \frac{M_{0P}^2}{32\pi^2 f_0^2}\log\frac{M_{0P}^2}{\mu^2}, \qquad P = \pi, K, \eta. \tag{5}$$

Note, however, that all the quark mass dependence always appears through the leading order masses M_{0P}^2 defined in Eq. (2). As a matter of fact, this also happens in the ChPT amplitudes, which means that studying the quark mass dependence, keeping B_0 fixed, is nothing but studying the meson mass dependence. In practice, and in order to get rid of the B_0 constant, we will recast all our results in terms of masses normalized to their physical values:

$$\frac{\hat{m}}{\hat{m}_{\rm phys}} = \frac{M_{0\pi}^2}{M_{0\pi\,\rm phys}^2}, \tag{6}$$

$$\frac{m_s}{m_{s\,\rm phys}} = \frac{M_{0K}^2 - M_{0\pi}^2/2}{M_{0K\,\rm phys}^2 - M_{0\pi\,\rm phys}^2/2}. \tag{7}$$

Note that, from now on, a quantity with a "phys" subscript refers to the value of that quantity in the physical case. Thus, in this work we will change quark masses, that, using Eqs. (3)–(5), imply a change in meson masses, which are the ones appearing explicitly in the ChPT scattering amplitudes. There are many advantages in using meson masses as the variation parameter, since, contrary to quark masses that have a complicated and scale dependent definition on the QCD renormalization scheme, meson masses are observables, with no scale dependence and a straightforward physical interpretation. Actually, many lattice results are also recast in terms of pion or kaon mass variations. Unfortunately the simple relations in Eqs. (6) and (7) are exact only when written in terms of the leading order masses M_{0P}, not the observable ones. Nevertheless, the one-loop corrections become numerically small when taking ratios so that, to a good degree of approximation, the reader still can think in terms of physical meson masses instead of their leading order values. Actually, in Fig. 1 we show that within the range of quark mass variations that we will consider in this work, the naive, but intuitive, relations

$$\frac{\hat{m}}{\hat{m}_{\rm phys}} \simeq \frac{M_\pi^2}{M_{\pi\,\rm phys}^2}, \quad \text{keeping } m_s = m_{s\,\rm phys}, \tag{8}$$

$$\frac{m_s}{m_{s\,\rm phys}} \simeq \frac{M_K^2}{M_{K\,\rm phys}^2}, \quad \text{keeping } \hat{m} = \hat{m}_{\rm phys} \tag{9}$$

are a very good approximation—within less than 10% error—to the correct ratios in Eqs. (6) and (7) that we actually use. To make our presentation of the results more intuitive we will give, when possible, our results both in terms of quark mass variation and the corresponding meson mass variation. At this point we have to address the question of how much we can vary the quark masses before our approach breaks down. First we want the pion

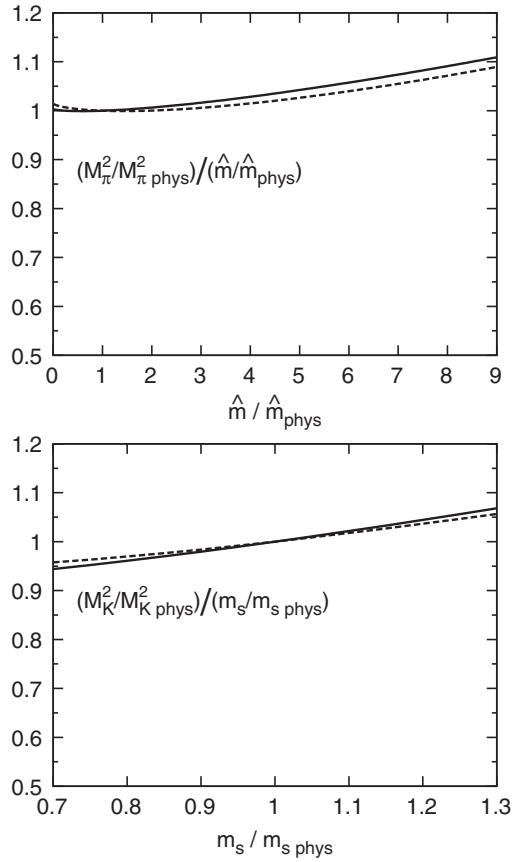

FIG. 1. Top panel: The ratio $(M_\pi^2/M_{\pi\,\rm phys}^2)/(\hat{m}/\hat{m}_{\rm phys})$; bottom panel: $(M_K^2/M_{K\,\rm phys}^2)/(m_s/m_{s\,\rm phys})$. Within the range of variation of this work, a relative variation of a quark mass can be also understood as the same relative variation in the corresponding meson mass squared to within ~10% accuracy. The continuous and dashed lines correspond to fit I and II sets of LECs given in Table I.

always lighter than the kaon and eta since otherwise the elastic approximation would make no sense for $\pi\pi$ or $K\pi$ scattering. Second, ChPT seems to work for masses as high as 500 MeV, since we already know that it provides a fairly good description of low energy $K\pi$ scattering, even though $M_K \sim 500$ MeV. Thus, when changing the nonstrange quark mass, keeping m_s fixed, we will show results up to $M_\pi < 440$ MeV but not beyond, since then $M_K \simeq 600$ MeV. Equivalently, this means $\hat{m}/\hat{m}_{\rm phys} \leq 9$. Concerning the strange quark variation with $\hat{m}$ fixed, we will consider $0.7 < m_s/m_{s\,\rm phys} < 1.3$, since M_π barely changes and 400 MeV $< M_K <$ 585 MeV. This ensures that the $m_K + m_\eta$ is not below the m_{K^*} mass so that we would need a coupled channel formalism. Of course, the closer to the estimated applicability limits the less reliable our formalism will be. The SU(3) $\pi\pi$ and $K\pi$ one-loop amplitudes were first calculated in [11], although for technical reasons explained in [12] needed for the implementation of exact unitarity later on, we use the expressions in the appendix of [12], but written in terms of all physical constants M_π, M_K, M_η, f_π, f_K, f_η as explained in [10]. For completeness we show here the decay constant dependence on meson masses.

$$
\begin{aligned}
f_\pi &= f_0\Big[1 - 2\mu_\pi - \mu_K + \frac{4M_{0\pi}^2}{f_0^2}(L_4^r + L_5^r) + \frac{8M_{0K}^2}{f_0^2}L_4^r\Big],\\
f_K &= f_0\Big[1 - \frac{3\mu_\pi}{4} - \frac{3\mu_K}{2} - \frac{3\mu_\eta}{4} + \frac{4M_{0\pi}^2}{f_0^2}L_4^r\\
&\quad + \frac{4M_{0K}^2}{f_0^2}(2L_4^r + L_5^r)\Big],\\
f_\eta &= f_0\Big[1 - 3\mu_K + \frac{4L_4^r}{f_0^2}(M_{0\pi}^2 + 2M_{0K}^2) + \frac{4M_{0\eta}^2}{f_0^2}L_5^r\Big].
\end{aligned}
\tag{10}
$$

Of course, for $\pi\pi$ and $K\pi$ elastic scattering the most relevant quark mass dependence comes via M_π, M_K and f_π, f_K (since etas only appear in loops). Consequently, the LECs that play the most important role are L_4, L_5, L_6, and L_8, since they appear in Lagrangian terms that contain explicitly powers of the quark mass matrix. In contrast, the Lagrangian terms proportional to the L_1, L_2, and L_3 constants only contain derivatives and thus are somewhat less relevant for the quark mass dependence, but more relevant in terms of s dependence. Finally, let us remark that despite the fact that their effect is encoded in the LECs, the ChPT amplitudes, being an expansion, cannot describe resonances and their associated poles in the second Riemann sheet. Actually, resonances are usually identified with a saturation of the unitarity constraints, which for elastic partial waves of definite isospin I and angular momentum J read

$$
\mathrm{Im}\, t_{IJ}(s) = \sigma(s)|t_{IJ}(s)|^2 \Rightarrow |t_{IJ}(s)| \leq 1/\sigma(s), \tag{11}
$$

where $\sigma(s) = 2k/\sqrt{s}$ and k is the center of mass momentum. The above equations imply that the partial wave can be recast in terms of a single phase or ''phase shift'':

$$
t_{IJ}(s) = \exp i\delta_{IJ}(s) \sin\delta_{IJ}(s)/\sigma(s). \tag{12}
$$

In this work we are only interested in the $(I, J) = (0, 0)$, (1, 1), and (2, 0) channels for $\pi\pi$ scattering and $(I, J) = (1/2, 0)$, $(1/2, 1)$, and $(3/2, 0)$ for πK scattering. For simplicity we will drop the IJ subindex when discussing general properties of elastic partial waves. Note, however, that the ChPT expansion Eq. (1), being basically a polynomial in energy, violates the bound in Eq. (11) as the energy increases and cannot generate poles. Still, ChPT satisfies elastic unitarity perturbatively:

$$
\mathrm{Im}\, t_2(s) = 0, \qquad \mathrm{Im} t_4(s) = \sigma|t_2(s)|^2, \ldots. \tag{13}
$$

But, of course, elastic unitarity can be badly violated if the ChPT series is extrapolated close to a resonance. For these reasons, the resonance region lies beyond the reach of standard ChPT. However, we will see next that ChPT can be used in an alternative way.

B. Dispersion relations, unitarity, and ChPT

Instead of simply extrapolating its series to higher energies, ChPT can be used to calculate the subtraction constants of a dispersion relation for the two-body amplitude. These constants correspond to the values of the amplitude or its derivatives at a low energy point where the use of ChPT is well justified. The remaining information to build the amplitude comes from the strong constraints of analyticity and unitarity.

First of all, it is straightforward to rewrite the strong nonlinear elastic unitarity constraint given in Eq. (11), as follows:

$$
\mathrm{Im}\, 1/t(s) = -\sigma(s). \tag{14}
$$

This means that, from unitarity, we know *exactly* the imaginary part of $1/t$ in the elastic region. We are only left to determine the real part of $1/t$.

Concerning the analyticity constraints, for simplicity let us consider first the case of two identical particles, as in $\pi\pi$ scattering. Then, the analytic structure in the complex s plane is rather simple: it has a ''right'' or ''physical'' cut on the real axis from threshold to $+\infty$, and a ''left'' cut from $-\infty$ to $s = 0$. By means of the Cauchy theorem, a dispersion relation provides the amplitude anywhere inside the cut complex plane in terms of a weighted integral of its imaginary part over the cuts.

In our case, instead of t we are interested in a dispersion relation for $1/t$ since we know exactly its imaginary part in the elastic region thanks to Eq. (14). For convenience, and since t_2 is real, instead of $1/t$ we define $G = t_2^2/t$, that also has a right cut (RC) and a left cut (LC). Since scalar waves are known to have dynamical Adler zeros in the low energy region below threshold, we will also allow for a pole

contribution PC in $G(s)$. All in all, we can write a dispersion relation for $G(s)$ as follows:

$$G(s) = G(0) + G'(0)s + \frac{1}{2}G''(0)s^2 + \frac{s^3}{\pi} \times \int_{RC} ds' \frac{\mathrm{Im}G(s')}{s'^3(s'-s)} + LC(G) + PC. \quad (15)$$

In the elastic region, unitarity in Eq. (11), together with Eq. (13), allows us to evaluate exactly $\mathrm{Im}G = -\sigma t_2^2 = -\mathrm{Im}t_4$ on the RC. Note the three $1/s'$ factors—called subtractions—that we have introduced to suppress the high energy part and, in particular, the inelastic contributions, so that the integrals are dominated by the low energy region. But once the integrals are dominated by the low energy, it is well justified to use ChPT inside the integrals and thus, for instance, the LC integral to one loop ChPT is given by $LC(G) \simeq LC(-t_4) + \cdots$.

The price to pay for the three subtractions is that analyticity only determines the function up to a second order polynomial $G(0) + G'(0)s + \frac{1}{2}G''(0)s^2$. However, note that its coefficients correspond to the values of the amplitude or its derivatives at $s = 0$, where ChPT can be safely applied. In particular, to one loop, $G(0) \simeq t_2(0) - t_4(0)$, $G'(0) \simeq t_2'(0) - t_4'(0)$, and $G''(0) = -t_4''(0)$, since $t_2''(0)$ vanishes. Let us neglect for the moment the pole contribution, which is of higher order and only numerically relevant below threshold. Then one finds that all contributions can be recast in terms of the leading $t_2(s)$ and next-to-leading $t_4(s)$ ChPT amplitudes. Finally, we arrive at the so-called inverse amplitude method (IAM) [13,14]:

$$t(s) \simeq \frac{t_2^2(s)}{t_2(s) - t_4(s)}. \quad (16)$$

Remarkably, this simple equation ensures elastic unitarity, matches ChPT at low energies, and, using LECs compatible with existing determinations, describes fairly well data up to somewhat less than 1 GeV, generating the ρ, K^*, σ, and κ resonances as poles on the second Riemann sheet. It has been shown [15] that the scalars can actually be generated mimicking the LEC, tadpole, and crossed channel diagrams by a cutoff of natural size, and thus it is said that scalars are ''dynamically generated'' from, essentially, meson-meson dynamics (meson loops). In contrast, to generate the vectors, a precise knowledge of the LECs is needed, namely, of the underlying, non-meson-meson QCD dynamics.

Here we will update this description of experimental data but furthermore we will simultaneously describe the existing lattice results for decay constants and some scattering lengths.

The IAM equation above is just the one-loop result, but it can be easily and systematically extended to higher orders of ChPT or generalized within a coupled channel formalism [10,12,16], generating also the $a_0(980)$, $f_0(980)$ and the octet ϕ. However note that there is no dispersive justification for the coupled channel approach formula[1] and that is the main reason, apart from simplicity, why we have restricted our analysis to the elastic case.

For completeness, and even though it will be negligible except for very high masses near the applicability limits of our approach, let us now include the pole contribution PC ignored so far. Its contribution can be calculated explicitly from its residue [17] and, to one loop, we find a modified IAM (mIAM) formula:

$$t^{\mathrm{mIAM}} = \frac{t_2^2}{t_2 - t_4 + A^{\mathrm{mIAM}}},$$
$$A^{\mathrm{mIAM}} = t_4(s_2) - \frac{(s_2 - s_A)(s - s_2)[t_2'(s_2) - t_4'(s_2)]}{s - s_A}, \quad (17)$$

where s_A is the position of the Adler zero in the s plane, and s_2 its LO approximation. The standard IAM is recovered for $A^{\mathrm{mIAM}} = 0$, which holds exactly for all partial waves except the scalar ones. Above, and in the usual IAM derivation [14] A^{mIAM} was neglected, since it formally yields a next-to-next-to-leading-order (NNLO) contribution and is numerically very small, except near the Adler zero, where it diverges. However, if A^{mIAM} is neglected, the IAM Adler zero occurs at s_2, correct only to LO, it is a double zero instead of a simple one, and a spurious pole of the amplitude appears close to the Adler zero. All of these caveats are removed with the mIAM, Eq. (17). The differences in the physical and resonance region between the IAM and the mIAM are less than 1%. However, as we will see, for large M_π the σ and κ poles ''split'' into two virtual poles below threshold, one of them moving toward zero and approaching the Adler zero region, where the IAM fails. Thus, we will use for our calculations the mIAM, although it is only relevant for the mentioned second σ and κ poles, and only when they are very close to their corresponding Adler zeros.

Finally, we want to comment on the unequal mass case, since we also want to describe $K\pi$ elastic scattering. The main difference now is that the left cut extends from $-\infty$ to $s = (M_1 - M_2)^2$, and also that there is a circular cut, centered at $s = 0$ with radius $|M_1^2 - M_2^2|$. Again their main contribution comes from a region where ChPT can be applied. This time, however, $t_2(s)$ has *two* zeros instead of one,

$$s_{2\pm} = \tfrac{1}{5}(M_K^2 + M_\pi^2 \pm 2\sqrt{4M_K^4 - 7M_K^2M_\pi^2 + 4M_\pi^4}),$$

and the modification to the IAM reads

[1]If we followed a similar approach the left cuts would mix when calculating the inverse matrix and produce spurious analytic structures.

$$A^{\mathrm{mIAM}}(s) = \frac{t_2(s)^2}{t_2'(s_{2+})^2}\left[\frac{t_4(s_{2+})}{(s-s_{2+})^2} - \frac{(s_{2+}-s_A)}{(s-s_{2+})(s-s_A)} \times \left(t_2'(s_{2+}) - t_4'(s_{2+}) + \frac{t_4(s_{2+})t_2''(s_{2+})}{t_2'(s_{2+})}\right)\right]. \tag{18}$$

Once again we note that this modification will be numerically negligible except in the close vicinity of the Adler zero. The poles of the resonances under study will only come close to that region for very high values of the quark masses, in the limit of applicability of ChPT and our approach.

Before describing our fits, we want to remark that, in the IAM derivation above, ChPT does not play any role outside its applicability limits. By including three subtractions we have suppressed strongly all contributions to the integrals in high energy regions where ChPT results are not reliable. Finally, the three subtraction constants, which correspond to values of the amplitudes or their derivatives at $s = 0$ are well calculated with ChPT. Of course, this is just a one-loop calculation, although the generalization to higher orders is tedious but straightforward. Hence, our approach does not model the left or inelastic cuts, but just uses the corresponding ChPT approximation that, in principle, can be improved order by order, eventually including more subtractions.

II. FITS TO DATA AND LATTICE RESULTS

As commented before, it has been known for a long time [14] that with the one-loop elastic IAM (the mIAM is almost identical) in Eq. (16) it is possible to obtain a remarkable description of $\pi\pi$ and $K\pi$ experimental data up to somewhere below 1 GeV. Simultaneously, the IAM generates the poles associated to the $f_0(600)$, $\rho(770)$, $K^*(892)$, and $\kappa(800)$ resonances and this is achieved using parameters compatible with those of standard ChPT [12]. However, that description was obtained from a fit to experimental data, and therefore it is mostly sensitive to the LECs L_1, L_2, L_3 that predominantly govern the s dependence of partial waves, but much less so to the rest of the LECs that carry an explicit meson mass dependence. Of course, since now we want to extrapolate the IAM fits to nonphysical masses, it is very important that we use a good description of the mass dependence in observables like masses, decay constants, etc. before extracting conclusions about resonance behavior. For that reason, we are presenting here an updated IAM description of experimental data simultaneously fitted to the available lattice results on the mass dependence of M_π/f_π, M_π/f_K, and M_K/f_K as well as scattering lengths for the doubly charged channel in $\pi\pi$, $K\pi$, and KK scattering. Note that for the moment, these lattice data are only available in the highest isospin combination for each particle pair.

In order to change the masses and decay constants according to Eqs. (3)–(5) and (10), we need first to extract the tree level quantities: $M_{0\pi}^2$, M_{0K}^2, and f_0 from the physical values of the pion, kaon, and eta masses as well as the three decay constants f_π, f_K, and f_η. Note that $M_{0\eta}^2$ will be obtained from the Gell-Mann-Okubo relation: $4M_{0K}^2 - M_{0\pi}^2 - 3M_{0\eta}^2 = 0$. Since there are more physical values than tree level constants, for a given set of LECs we actually use the tree level constants that best fit the physical ones. Thus, the physical masses and decay constants that we will obtain when recovering them from the tree level ones will be only approximate. This is, of course, the consequence of using a truncated expansion—ChPT to one loop—to describe observables.

We have made two fits whose resulting LEC sets are given in the two last columns of Table I. Since there are many parameters, there are strong correlations. Thus, sets with quite different parameters can give raise to acceptable descriptions of data, depending on how one weights experiment and lattice results. On fit I we have fitted to experimental data coming from [18] and to lattice results given in [19]. Despite we show in Fig. 1 these data, for the $(I, J) = (0, 0)$ and $(2, 0)$ waves, where many different experiments are actually incompatible, we have fitted to the phase shifts arising from the dispersive analysis of the experimental data in [20], where a complete set of forward dispersion relations and Roy equations was constrained on a phenomenological fit to all waves. For the (1, 1) wave we have used also the phenomenological phase shifts from that solution since, apart from the dispersive constraints, it fits the data of the electromagnetic form factor of the pion, which is much more reliable and precise than the existing experiments on (1, 1) pion-pion scattering. Anyway, since for πK and other waves we are still using scattering, and also because the method has an intrinsic error due to the NLO approximation on the integrals, we have added in quadrature to the experimental data errors a constant error of 2 degrees and a variable error of 5% of the phase shift and to lattice results on masses over decay constants 5% of their values also in quadrature to their errors. We have also introduced a constraint so that the LECs do not differ much from those found in the K_{l4} analysis to two loops of [8], by weighting also in the χ^2 the LECs with the values in [8]. On fit II we have given an additional weight to the large $1/N_c$ constraint $2L_1 - L_2 = 0$ (dividing its error by 10 when calculating the χ^2) whereas we have relaxed the constrains on δ_{11} and $\delta_{1/20}$ (dividing their χ^2 by 1.5).

For comparison, also in Table I we provide three typical sets of LECs available in the literature obtained from data analyses using dispersive techniques plus ChPT. Those on the first and the second columns come from a one- and two-loop analysis of K_{l4} decays [8], where L_4 and L_6 were set equal to zero (following leading order $1/N_c$ arguments). The "Roy-Steiner" column comes from a dispersive analysis of πK scattering [9]. Note that the LECs in these

sets are frequently within more than 2 standard deviations from one another, and we consider that their difference is indicative of the typical size of systematic uncertainties in our knowledge of LECs. As commented above, since the one-loop IAM generates correctly only the s-channel leading logs of the two-loop calculation, which are dominant at low energies, it is not clear whether we should compare with the LECs obtained in the one- or two-loop ChPT analysis. Actually, all of our IAM LECs lie very close, or within the uncertainties, of at least one of the previous determinations given in the table. Taking into account the uncertainties in these nonunitarized determinations, we consider that the agreement between the IAM LECs and previous determinations is fair. Let us remark that the relevant fact about this comparison is to note that we do not need to make any fine-tuning of the LECs, like changing well-established signs, changing order of magnitude, etc., to describe the experimental and lattice data simultaneously.

Finally, we also provide in Table I, the IAM III set of LECs, which corresponds to one of the three fits obtained using the coupled channel IAM in [10]. This set was fitted to experimental data only and the uncertainties quoted are just statistical. Taking into account that we are using the single channel IAM instead of the coupled channel one, and the estimate of systematic uncertainties discussed above, we see that our new fits, including new experimental data and lattice results, are not too different from those already obtained in [10].

In Fig. 2 we show the results of our fits compared with experimental data on $\pi\pi$ and πK elastic scattering phase shifts. The best description is given by fit I (continuous line), whereas fit II gives a somewhat too heavy $\rho(770)$ vector resonance (by roughly 50 MeV, i.e., a 6% error). For comparison, we show as a dotted line the results of the IAM if we used the ChPT LECs obtained from the two-loop analysis of K_{l4} decays listed in Table I. We also show as a dot-dashed line the results that would be obtained if the nonunitarized ChPT one-loop results, using the same set of LECs, are extrapolated to higher energies. Note that the IAM results describe rather well both the resonant and nonresonant shapes up to 1 GeV or slightly above, except for the scalar-isoscalar δ_{00} that is only described up to 800 MeV. This is due to the presence of the sharp rise caused by the $f_0(980)$ resonance that decays mostly to two kaons and can only be described with the coupled channel

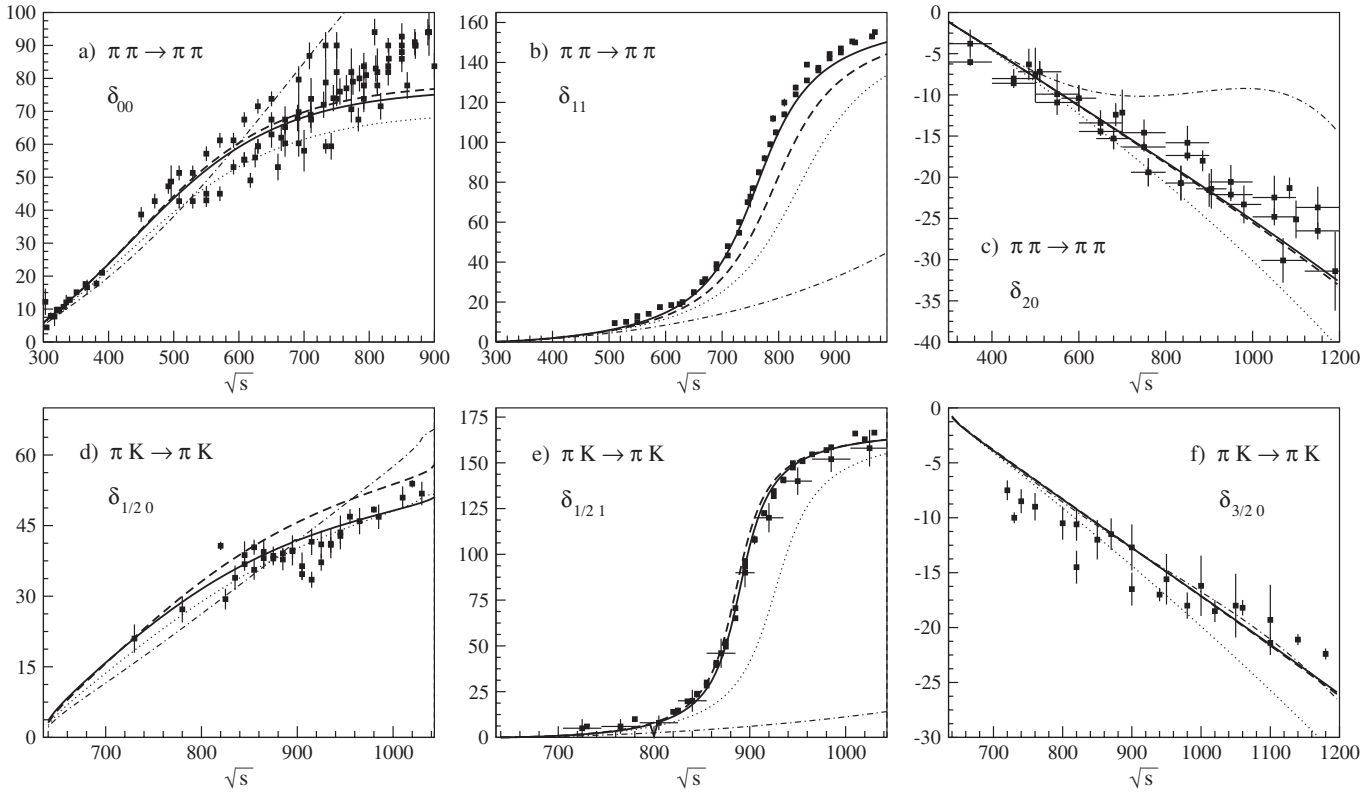

FIG. 2. Results of our IAM fits versus experimental data on $\pi\pi$ and πK scattering. The continuous and dashed lines correspond, respectively, to fits I and II, whose parameters are given in Table I. For comparison we show the results of the IAM if we used the ChPT LECs obtained from the two-loop analysis of K_{l4} decays listed also in Table I (dotted lines) as well as the results of standard nonunitarized ChPT with the same set of LECs (dot-dashed lines). The plotted data correspond to experimental results [18], which are often incompatible. For that reason, in our fits, and for $\pi\pi$ scattering, we have actually used the results of a dispersive analysis of these data [20].

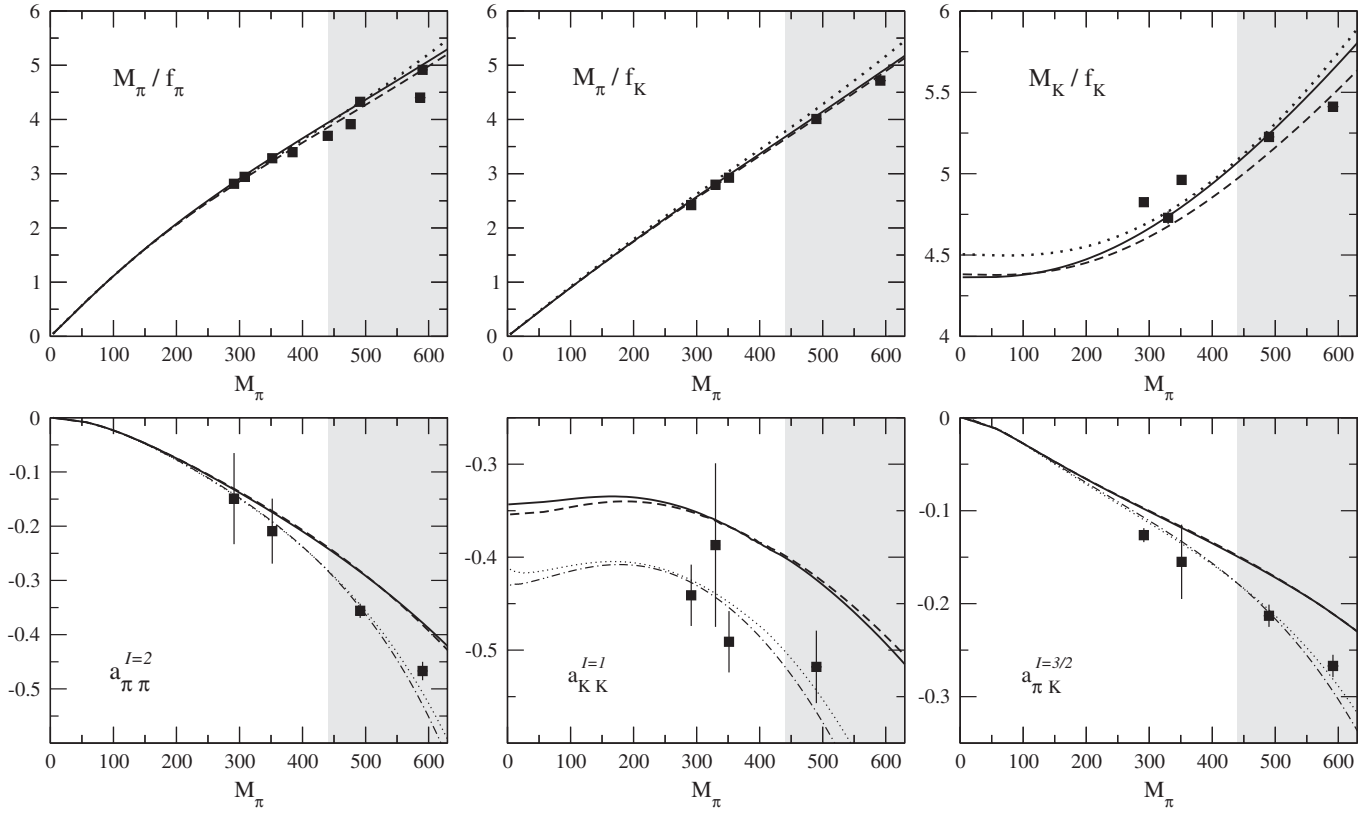

FIG. 3. Result of the unitarized fits to lattice calculations of M_π/f_π, M_π/f_K, M_K/f_K and the $\pi^+\pi^+$, K^+K^+, $K^+\pi^+$ scattering lengths. The continuous and dashed lines correspond, respectively, to fits I and II, whose parameters are given in Table I. For comparison we show the results of the IAM if we used the ChPT LECs obtained from the two-loop analysis of K_{l4} decays listed also in Table I (dotted lines) as well as the results of standard nonunitarized ChPT with the same set of LECs (dot-dashed lines). Lattice results come from [19]. The gray area lies beyond our applicability region; however, it is useful to check that our description does not deteriorate too rapidly.

IAM formalism, [10,12,16], that we do not use here for the reasons explained above.

Those results are, of course, well known, and these fits would just be an update of [10] if we had not also included lattice data on the fit that we show in Fig. 3. Note that we are fitting results on M_π/f_π, M_π/f_K, and M_K/f_K and the $\pi^+\pi^+$, K^+K^+, and $K^+\pi^+$ scattering lengths [19]. Once again we show fits I and II as continuous and dashed lines, respectively, together with IAM results using the LECs from a two-loop analysis of K_{l4} decays listed in Table I (dotted line) and nonunitarized ChPT to one loop with the same set of LECs (dot-dashed line). As explained above, we do not consider that our method should be trusted for pion masses heavier than 440 MeV, being optimistic, and that is why the heavier mass region is shown as a gray area.

III. DEPENDENCE ON *u* AND *d* QUARK MASSES

Now that we have a good description of both the energy dependence of pion-pion amplitudes together with the mass dependence of the few observables available from lattice, we can change the value of the light quark mass, keeping m_s fixed, and predict the behavior of the resonances generated within the IAM.

A. Light vector mesons: The $\rho(770)$ and $K^*(892)$

The $\rho(770)$ and $K^*(892)$ vector resonances are well-established $q\bar{q}$ states belonging to an SU(3) octet. The first is produced in $\pi\pi$ scattering, and its quark mass dependence was already studied within SU(2) ChPT [3]. Here we will just check that we reobtain very similar results within the SU(3) formalism, while describing simultaneously the lattice observables shown in Fig. 3. However, the $K^*(892)$ appears in πK scattering and can only be obtained using SU(3) ChPT as we do here.

1. Mass and width

Thus, in Fig. 4, we show the dependence of the light vector resonances on the nonstrange quark masses, using one-loop SU(3) ChPT unitarized with the IAM. For each resonance, these masses and widths are defined from the position of their associated pole in the second Riemann sheet, through the usual Breit-Wigner identification: $\sqrt{s_{\rm pole}} \equiv M - i\Gamma/2$. We show the results for fits I and II

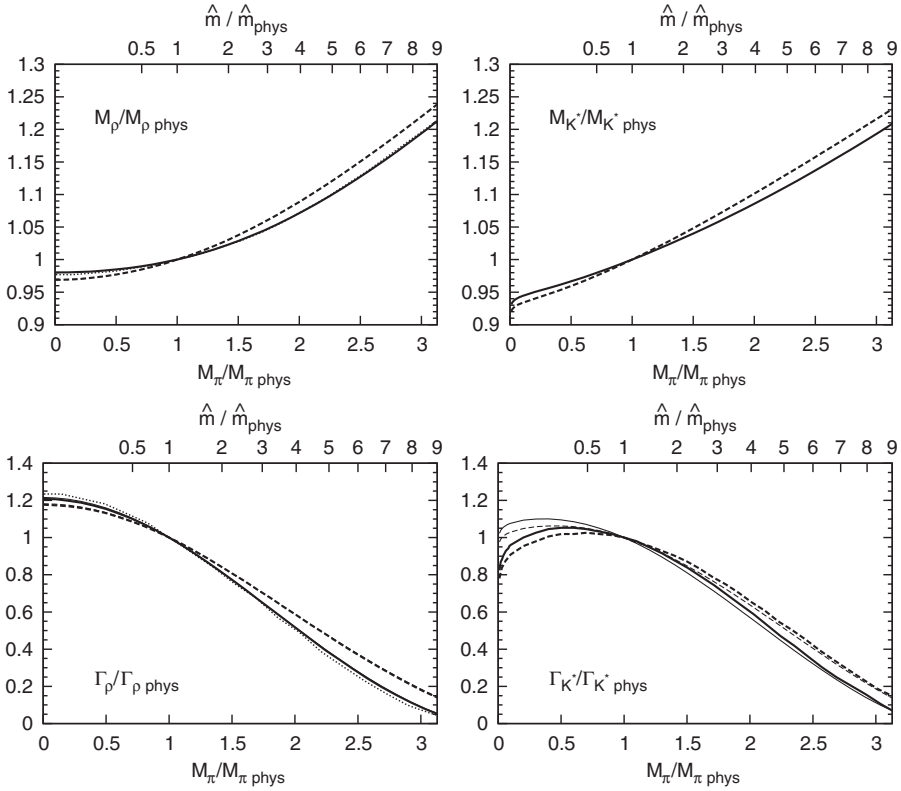

FIG. 4. Dependence of the $\rho(770)$ and $K^*(892)$ mass and width with respect to the nonstrange quark mass $\hat{m}$ (horizontal upper scale), or the pion mass (horizontal lower scale). Note that we give all quantities normalized to their physical values. The thick continuous and dashed lines correspond, respectively, to fits I and II described in the text with unitarized SU(3) ChPT. For the ρ these results are very compatible with those in [3] using SU(2) ChPT (dotted lines). The continuous (dashed) thin line shows the M_π dependence of the widths from the change of phase space only, assuming a constant coupling of the resonances to two mesons, $\rho(770)$ to $\pi\pi$ and $K^*(892)$ to πK, calculated from the dependence of masses and momenta given by fit I (II). For the $\rho(770)$ the thin and dashed lines overlap completely.

as continuous and dashed lines, respectively. The results for both fits are very consistent and their difference can be taken as an estimation for systematic uncertainties in the choice of LECs. To suppress *systematic uncertainties* we give all quantities normalized to their physical values. Note that we provide two scales for the mass variation: In the upper horizontal axis, we show the variation of the quark mass in terms of $\hat{m}/\hat{m}^{\rm phys}$, whereas in the lower horizontal axis we show the variation of the pion mass in terms of $M_\pi/M_\pi^{\rm phys}$. The one-loop ChPT relation between these two scales is given by Eqs. (2) and (3). To be precise, this relation changes for different LECs, but, as we already showed in Fig. 1, the difference is too small to be observed with the naked eye in the axes of Fig. 4.

In the left panels we also show, as a dotted line, the SU(2) ChPT result already obtained in [3], which is fairly consistent with the new SU(3) results. Of course, the difference is somewhat larger when the pion mass is closer to the kaon mass, and the kaons start playing a more prominent role. Of course, since the SU(2) results [3] already described fairly well the available lattice calculations for the $\rho(770)$ mass, so it happens with the SU(3) results here. In addition, this ensures that the M_ρ dependence on M_π agrees nicely with the estimations for the two first coefficients of its chiral expansion [21], which was already checked in the SU(2) case [3].

Since the vertical scale is the same for the $\rho(770)$ and $K^*(892)$ plots, the similarity of their behavior is very evident. Both their masses increase smoothly as the quark mass increases, but much slower than the pion mass. Some differences can be observed for small $\hat{m}$, but this is due to the fact that the SU(3) breaking between the $\rho(770)$ and the $K^*(892)$ is more evident since we keep m_s fixed to its large physical value. What is interesting to observe is that the naive rule of thumb frequently used in the literature [22], that $\partial M_R/\partial\hat{m} = N_R^v$, where N_R^v is the number of valence nonstrange quarks, yields the correct order of magnitude (and this is how it has been used in [22]) but would predict a 2:1 relation for the slope of the $\rho(770)$ with respect to that of the $K^*(892)$, which is not observed for light quarks.

Continuing with our analysis, we note that, as the quark mass increases, the two-pion and pion-kaon threshold grow faster than the masses of the resonances and, as a consequence, there is a strong phase space suppression than can

account exclusively for the decrease of their widths. We show in the lower panels the M_π dependence of Γ_ρ and Γ_{K^*} normalized to their physical values. The decrease of the widths is largely kinematical, following remarkably well the expected reduction from phase space as the masses of the NGB increase [thin continuous and dashed lines corresponding to fits I and II, respectively, although for the $\rho(770)$ they overlap so well that the thin lines are not seen]. This result was already found for the $\rho(770)$ within the SU(2) formalism and is nicely confirmed here. This suggests that there is no dynamical effect through the vector coupling to two mesons, as we will analyze next.

2. Coupling to two mesons

The dynamics of resonance-meson-meson interaction is encoded in the coupling constant that we obtain from the residue of the amplitude at the pole position as follows:

$$g^2 = -16\pi \lim_{s\to s_{\rm pole}} (s - s_{\rm pole}) t(s) \frac{3}{4k^2}, \tag{19}$$

where the normalization factors are chosen to recover the usual expression for the two-meson width of narrow vector resonances:

$$\Gamma_V = |g|^2 \frac{1}{6\pi} \frac{|\mathbf{k}|^3}{M_V^2}, \tag{20}$$

$|\mathbf{k}|$ being the modulus of the meson three-momentum. Actually, by identifying $\sqrt{s_{\rm pole}} = M_V - i\Gamma_V$, we have explicitly checked that we obtain the same numerical value for the coupling with both equations. We find $|g_{\rho\pi\pi}| \simeq 6.1$ and $|g_{K^*\pi K}| \simeq 5.5$.

Then, in Fig. 5 we show the dependence of the $g_{\rho\pi\pi}$ (left panel) and the $g_{K^*\pi K}$ (right panel) couplings with respect to the pion mass (lower horizontal scale) or the nonstrange quark mass $\hat{m}$ (upper horizontal scale). In order to suppress systematic uncertainties, we have normalized the couplings to their physical values. Note that the $g_{\rho\pi\pi}$ is remarkably constant, deviating from its physical value by 2% at most, despite the fact that the quark mass is changed by a factor of 9. It is also relevant because it justifies the constancy assumption made in lattice studies of the $\rho(770)$ width [23]. The $g_{K^*\pi K}$ is also quite independent of the nonstrange quark mass, deviating by 10% at most in the chiral limit and by less than 4% when the quark mass is increased by a factor of 9. The results for fits I and II are almost indistinguishable.

The constancy of the vector-meson-meson couplings, together with the classic KSRF relation [24], provides a striking connection between the quark mass dependence of the rho mass and the pion decay constant. Actually, the KSRF relation, obtained from the partially conserved axial current and vector meson dominance, reads

$$g_{\rho\pi\pi}^2 \simeq M_\rho^2/8f_\pi^2. \tag{21}$$

Note that in our calculation we are obtaining M_ρ from a one-loop ChPT unitarized calculation, whereas f_π comes simply from the next-to-leading-order ChPT calculation, but, of course, without unitarization. It is therefore quite remarkable that the ratio M_ρ/f_π obtained from our amplitudes, shown in Fig. 6, is constant within less than 5% accuracy, when the quark mass varies by a factor of 9, or the pion mass by a factor of 3. Note that, as usual, in Fig. 6 we have normalized the ratio to its physical value. It seems that the simple KSRF relation holds remarkably well up to surprisingly large values of the nonstrange quark mass, and therefore the M_ρ quark mass dependence can be recast with the same factor as that for f_π.

A similar result is found for the $K^*(892)$ whose ratio M_{K^*}/f_π is also shown in Fig. 6 to deviate by less than 2% from its physical value. Note that, according to the second reference in [24], the f_K dependence does not show up in the relation. Actually, had we used $M_{K^*}/\sqrt{f_\pi f_K}$ instead, the deviation would have been a factor of 3 larger.

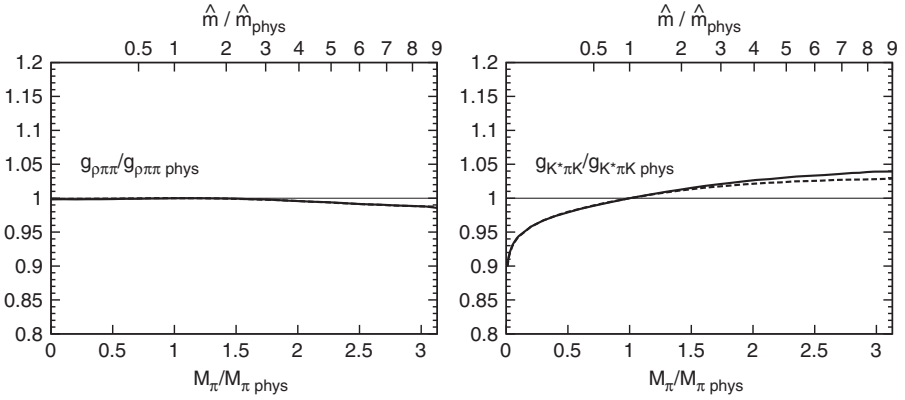

FIG. 5. Two-meson-vector coupling dependence with respect to the nonstrange quark mass $\hat{m}$ (horizontal upper scale), or the pion mass (horizontal lower scale). Note we normalize the couplings to their physical values. We show on the left the $\rho(770)$ coupling to two pions and on the right that of the $K^*(892)$ to πK (continuous and dashed lines correspond to fits I and II, respectively).

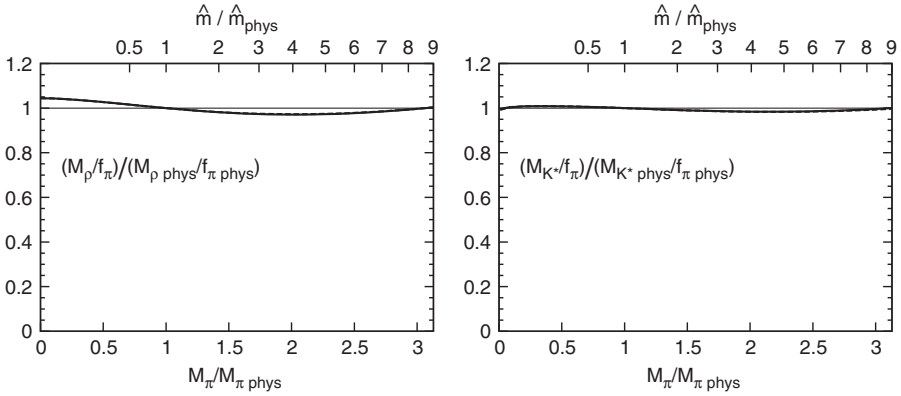

FIG. 6. Ratio of vector resonance masses to the pion decay constant dependence on the nonstrange quark mass (horizontal upper scale), or the pion mass (horizontal lower scale). Once again, we normalize all quantities to their physical values. We show the M_ρ/f_π on the left and M_{K^*}/f_π on the right (continuous and dashed lines correspond to fits I and II, respectively). Both masses seem to follow the f_π quark mass dependence up to less than 5% and 2%, respectively.

B. Light scalar mesons: The $f_0(600)$ and $\kappa(800)$

The $f_0(600)$, or sigma, and the $\kappa(800)$ scalar mesons are still somewhat controversial. The main problem is their huge width that makes their experimental identification complicated. Despite the fact that their pole mass and width has been determined by several groups with the help of model independent dispersive techniques (with and without ChPT input) and a fairly reasonable agreement (see [9,14,25] for recent determinations), they are still cited with extremely cautious and conservative estimates in the PDG [26]. Their nature is even more controversial, and as commented above, there are no present lattice calculations with realistic quark masses that could shed some light on the problem. It is therefore even more interesting to obtain predictions on their quark mass dependence. Compared with the vector case, there is an additional complication because now we do not necessarily expect a similar behavior between the $\kappa(800)$ and the $f_0(600)$, since although the former should belong to an SU(3) octet, the latter could be in the singlet, the octet, or have a significant mixture of both. As a matter of fact, there are indications that its singlet component is actually dominant [27,28].

1. Mass and width

As the data show in Fig. 2, the sigma and kappa resonances do not present a peak nor a Breit-Wigner shape in the meson-meson scattering $(I, J) = (0, 0)$ and $(1/2, 0)$ waves, respectively. Once again, these masses and widths are defined from the position of their associated pole in the second Riemann sheet, as follows: $\sqrt{s_{\rm pole}} \equiv M - i\Gamma/2$, but one should keep in mind that these scalar states do not present the typical Breit-Wigner shape, so there is no immediate equivalence of the mass in terms of a peak in the cross section or a time delay in the propagation.

In Fig. 7 we show the pole mass and width dependence of light scalar resonances on the nonstrange quark mass. As in Fig. 4, we show quantities normalized to their physical values and we provide two scales for the horizontal axis: $\hat{m}/\hat{m}_{\rm phys}$ (upper horizontal axis) and $M_\pi/M_{\pi\,\rm phys}$ (lower horizontal axis). Once again, the continuous line represents the results for fit I, the dashed line those of fit II, and the dotted line stands for the results of unitarized SU(2) ChPT for the $f_0(600)$. As before we find that the fits I and II are very consistent with each other, and, for the $f_0(600)$ also with the existing SU(2) calculation of [3].

The most prominent feature of the scalars behavior is the appearance of two branches for the mass as defined above, already observed for the σ in [3]. The reason is that for physical values of the quark mass, the poles associated with resonances appear as conjugated poles in the second Riemann sheet, i.e., there are poles at $\sqrt{s_{\rm pole}} \equiv M \pm i\Gamma/2$. Of course, only the one in the lowest half plane is continuous with the physical amplitude in the real axis, and this is the one responsible for the physical resonance. However, as the quark mass increases these poles move closer to the real axis until they join in a single pole below threshold, but still in the second Riemann sheet. If the quark mass is increased further, the poles split again but without leaving the real axis. The position of each one of these poles corresponds to each one of the branches that we show in the upper panels of Fig. 7.

Although this qualitative behavior is a well-known possibility for potentials in scalar channels, one-loop unitarized ChPT is predicting the quark mass value for which it occurs, which is a genuine prediction for QCD. For scalar-isoscalar $\pi\pi$ scattering it was already observed in the SU(2) case [3]. Here we are confirming this position when using SU(3) instead of SU(2) ChPT, but we see it also happening for the $\kappa(800)$, although the point at which it happens depends more on the set of LECs. For this reason, we think that the existence of this nonanalyticity of the $\kappa(800)$ pole is robust, but not so much the precise quark mass value where it occurs.

This ''apparent splitting'' cannot occur for higher partial waves since they all carry a k^{2J} factor that forces the

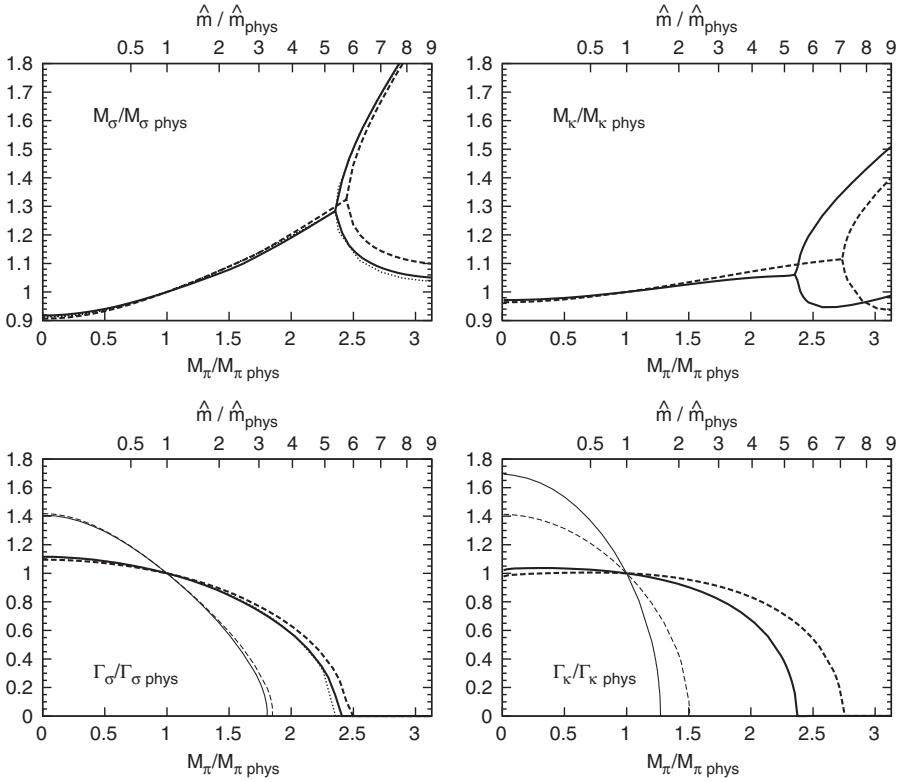

FIG. 7. Dependence of the $f_0(600)$ and $\kappa(800)$ mass and width with respect to the nonstrange quark mass $\hat{m}$ (horizontal upper scale), or the pion mass (horizontal lower scale). Note that we give all quantities normalized to their physical values. The thick continuous and dashed lines correspond, respectively, to fits I and II described in the text with unitarized SU(3) ChPT. For the $f_0(600)$ these results are very compatible with those in [3] using SU(2) ChPT (dotted lines). Let us remark that both resonances, being scalar, develop two poles on the real axis for sufficiently high masses. The thin lines show the decrease of the widths if it were only due to phase space reduction (the thin continuous lines correspond to fit I and the dashed ones to fit II).

conjugated poles to join the real axis exactly at threshold, and then one of them jumps to the first Riemann sheet.

Apart from the evident qualitative similarities between the behavior of the $f_0(600)$ and the kappa, it is also clear that quantitatively they behave somewhat differently. In particular, the growth of the $\kappa(800)$ mass before the ''splitting point'' is much softer than for the $f_0(600)$, and even softer than the $\rho(770)$ and $K^*(892)$ growth shown in Fig. 4 (please note the difference in scales between both figures).

In the lower panels of Fig. 7 we show the quark mass dependence of the sigma and kappa widths. On the left we show that the decrease of the sigma width we find with the SU(3) one-loop IAM is very consistent between fits I and II, and confirm the previous results within SU(2) [3]. On the right we show the results for the $\kappa(800)$ width. We also show that the width decrease for both of them cannot be attributed to the phase space reduction, due to the increase of pion and kaon masses, naively expected from the narrow width approximation

$$\Gamma_S = |g|^2 \frac{1}{8\pi} \frac{|p|}{M_S^2}, \tag{22}$$

which we show as a thin continuous (dashed) line corresponding to fit I (II). Despite the fact that the shape of the decrease is slightly different for the σ and κ, both scalars behave very differently than vector mesons. Actually, we will see next that this implies that the scalar couplings to two mesons have a much stronger quark mass dependence than the vector ones.

2. Coupling to two mesons

As we have just seen, the narrow width approximation in Eq. (22) above is of little use for scalars. But, of course, we can still extract the coupling constant from the residue as we did for vectors, although now the equation reads

$$g^2 = -16\pi \lim_{s \to s_{\rm pole}} (s - s_{\rm pole}) t(s). \tag{23}$$

We find $|g_{\sigma\pi\pi}| \simeq 2.86$ GeV and $|g_{\kappa\pi K}| \simeq 3.6$ GeV, to be compared to $|g_{\sigma\pi\pi}| \simeq 2.97 \pm 0.04$ GeV and $|g_{\kappa\pi K}| \simeq 4.94 \pm 0.07$ GeV, obtained in [28] or the $|g_{\sigma\pi\pi}| \simeq 2.2$ average obtained in [29]. The agreement is fairly reasonable, taking into account that the data that have been used, the σ and κ poles, and the models in those references differ substantially for each reference.

Thus, in Fig. 8 we show the quark mass dependence (upper horizontal scale) or pion mass dependence (lower

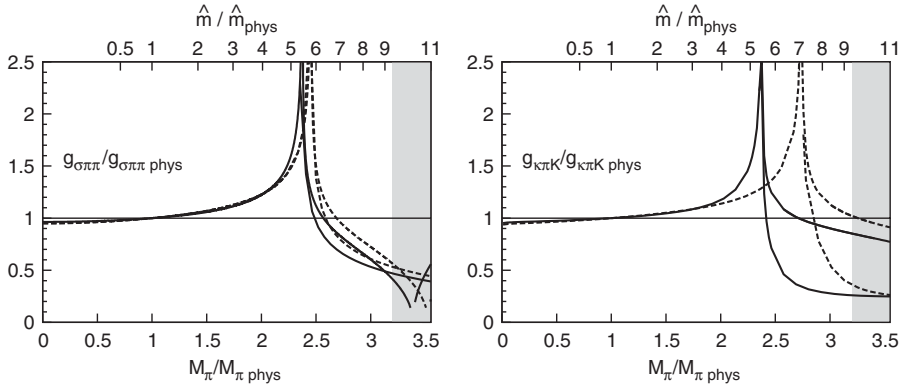

FIG. 8. Two-meson-scalar coupling dependence with respect to the nonstrange quark mass $\hat{m}$ (horizontal upper scale), or the pion mass (horizontal lower scale). Note we normalize the couplings to their physical values. We show on the left the $f_0(600)$ or sigma coupling to two pions and on the right that of the $\kappa(800)$ to πK. Let us remark that the two poles in the real axis show different couplings, which explains the doubling of the lines above the double branch point.

horizontal scale) of $g_{\sigma\pi\pi}$ and $g_{\kappa\pi K}$. As usual, all quantities are normalized to their physical values. Compared with Fig. 5 (note the different scales), we see that these couplings show a much stronger quark mass dependence. Moreover, they increase dramatically near the point of the apparent splitting. Beyond that point there are two nonconjugate poles lying on the real axis below threshold in the second Riemann sheet. For this reason, after the splitting point we plot two curves for each fit. The lowest curve corresponds to the pole closest to the threshold that eventually jumps into the first Riemann sheet. This threshold crossing from one sheet to the other corresponds to the point where the coupling tends to zero in the figures, in good agreement with the well-known result in [30]. Actually this can be checked numerically, because, as shown in [31] the coupling is inversely proportional to the energy derivative of the one-loop function [$G(s)$ in [31] and $J(s)$ in ChPT [12]], which is divergent at threshold. Despite this consistency check, within our approach this occurs at pion masses close to the naive applicability limit, and therefore the exact M_π value when this happens is not very reliable.

IV. DEPENDENCE ON THE STRANGE QUARK MASS

Up to here we have only been changing the values of the nonstrange quark mass keeping m_s fixed. However, since we are dealing with the full SU(3) ChPT formalism, we are now able to change the strange quark, keeping $\hat{m}$ fixed. The dependence of hadronic observables on the strange quark mass is also of interest for lattice studies and for cosmological considerations [6]. As we explained in Sec. I A we will only vary the strange quark mass in the limited range $0.7 < m_s/m_{s\,\mathrm{phys}} < 1.3$ to ensure that the kaon does not become too heavy to spoil the ChPT convergence nor too light to require a coupled channel formalism to deal with the $K^*(892)$ or $\kappa(800)$ resonances, thus introducing additional model dependences in our approach.

A. Light vector mesons: The $\rho(770)$ and $K^*(892)$

1. Mass and width

As in previous sections we define the mass and width of the vector resonances from the position of their associated poles. Thus, in the upper panels of Fig. 9 we show the quark mass dependence (or kaon mass dependence in the lower horizontal scale) of the ρ and $K^*(892)$ masses. In the lower panels we show the dependence of their widths. As usual, all quantities are normalized to their physical values to suppress systematic uncertainties.

As could be expected, both the mass and width of the $\rho(770)$, being nonstrange, are almost independent of the strange quark mass within the range of study. Note that the ρ mass actually decreases very slightly, by roughly 1%. Since the pion mass almost remains constant—see Eq. (3) and the L_6, L_4 values in Table I—this implies that phase space decreases slightly for smaller strange quark mass and the $\rho(770)$ width decreases accordingly. Actually, we can check in Fig. 9 that the width reduction follows remarkably well the phase space reduction expected from Eq. (20) (thin continuous and dashed lines).

Looking now at the right panels of Fig. 9, we notice that, as expected, the $K^*(892)$ shows a much stronger dependence than the $\rho(770)$ on the strange quark or the kaon masses. On the one hand, when the kaon mass is made lighter, the $K^*(892)$ mass decreases, as it happened when changing the light quark mass, although much faster, i.e., up to 5% when the kaon mass decreases by 20%. Nevertheless, and contrary to what happened when reducing $\hat{m}$, the $K^*(892)$ width increases significantly, up to 40%. This is due to the fact that the $K^*(892)$ decays to πK, but the kaon mass decrease is faster than that of the $K^*(892)$. On the other hand, when the kaon mass is made heavier, the $K^*(892)$ mass grows, but much slower than the kaon mass, so that phase space shrinks and the resonance width decreases once more. We are also showing as thin lines the expected variation of the widths if their only quark mass dependence came from the change in the particles

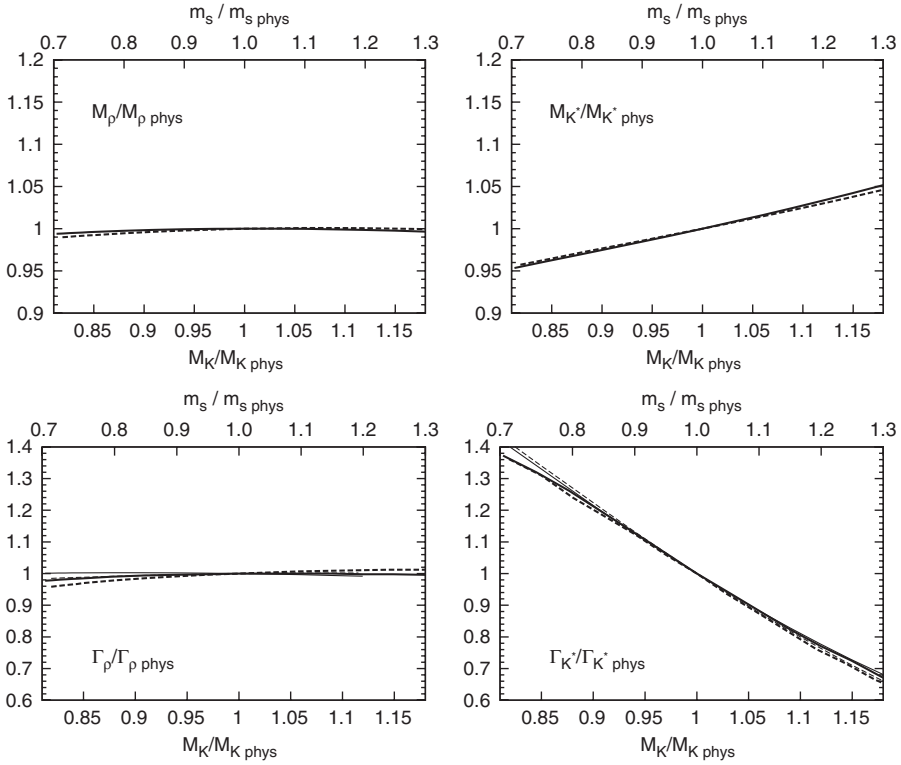

FIG. 9. Dependence of the $\rho(770)$ and $K^*(892)$ mass and width with respect to the strange quark mass m_s (horizontal upper scale), or the kaon mass (horizontal lower scale). Note that we give all quantities normalized to their physical values. The thick continuous and dashed lines correspond, respectively, to fits I and II described in the text with unitarized SU(3) ChPT. The thin lines show the decrease of the widths as if it were only due to phase space reduction (the thin continuous lines correspond to fit I and the dashed ones to fit II).

masses and the naive phase space suppression in Eq. (20) (thin continuous lines for fit I and thin dashed lines for fit II). We see that they are in very good agreement with our results from the IAM, which suggest that their coupling to two mesons is almost independent of the quark masses, which we will see next.

2. Coupling to two mesons

Thus, in Fig. 10 we show the dependence both on m_s and kaon masses of the vector to meson-meson couplings. As usual everything is normalized to their physical values. It can be noted that within the range of variation under study, which is 30% for the strange quark mass in either direction, both the $g_{\rho\pi\pi}$ and $g_{K^*\pi K}$ couplings change by 1% at most.

In Fig. 11 we show the results for the KSRF relation variation in terms of the strange quark mass. Since the ρ coupling has virtually no dependence on m_s, the relation remains trivially constant. For the $K^*(892)$ the relation is well satisfied (to within less than 5% from the physical value) in the whole m_s range of our study.

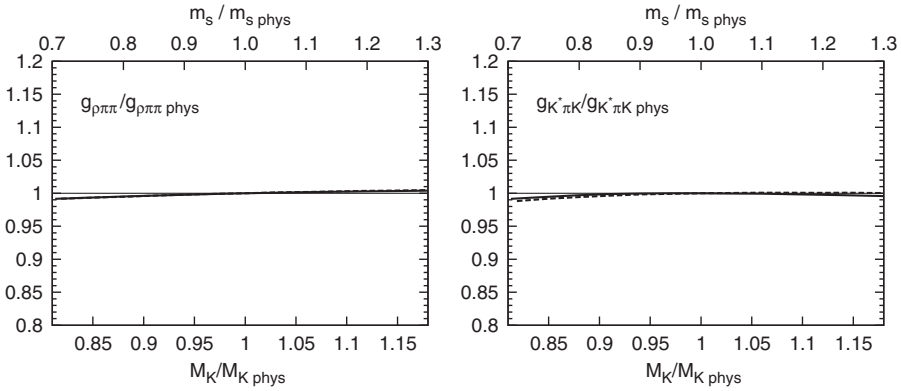

FIG. 10. Two-meson-vector coupling dependence with respect to the strange quark mass m_s (horizontal upper scale), or the kaon mass (horizontal lower scale). Note we normalize the couplings to their physical values. We show on the left the $\rho(770)$ coupling to two pions and on the right that of the $K^*(892)$ to πK.

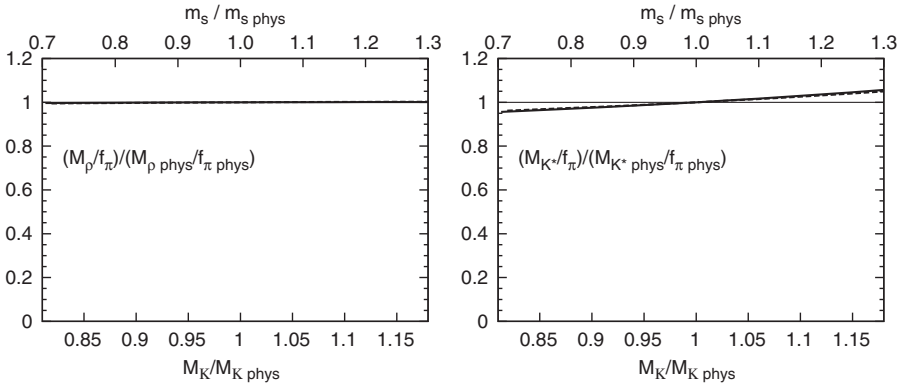

FIG. 11. Ratio of vector resonance masses to the pion decay constant dependence on the strange quark mass (horizontal upper scale), or the kaon mass (horizontal lower scale). Once again, we normalize all quantities to their physical values. We show the M_ρ/f_π on the left and M_{K^*}/f_π on the right (continuous and dashed lines correspond to fits I and II, respectively). For the ρ the result is trivial since we have already shown that its coupling does not depend on m_s. However the $K^*(892)$ mass deviates from the f_π quark mass dependence by less than 5% with respect to the physical value.

B. Light scalar mesons: The $f_0(600)$ and $\kappa(800)$

We simply repeat the procedure we used to study the light quark variation in Sec. III B, but this time changing the strange quark mass instead, and keeping $\hat{m}$ fixed.

1. Mass and width

Thus, in Fig. 12, we show the variation of the sigma and $\kappa(800)$ masses and widths with respect to the kaon mass variation (lower horizontal scale) or the strange quark mass (upper horizontal scale). Once again all masses are normalized to their physical values. As could be expected, we see in the left panels that the change on the sigma is smaller than 1% on both mass and width (beware we have changed the scale with respect to the previous Fig. 7 to make the changes more visible).

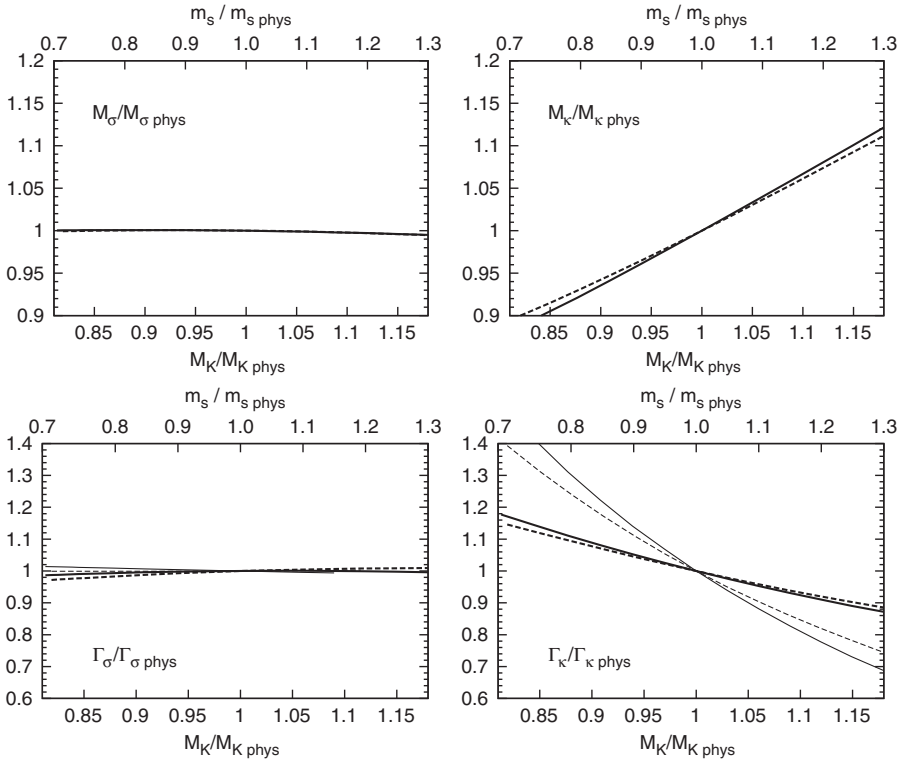

FIG. 12. Dependence of the $f_0(600)$ and $\kappa(800)$ mass and width with respect to the strange quark mass m_s (horizontal upper scale), or the kaon mass (horizontal lower scale). Note that we give all quantities normalized to their physical values. The thick continuous and dashed lines correspond, respectively, to fits I and II described in the text with unitarized SU(3) ChPT. The thin lines show the decrease of the widths as if it were only due to phase space reduction (the thin continuous lines correspond to fit I and the dashed ones to fit II).

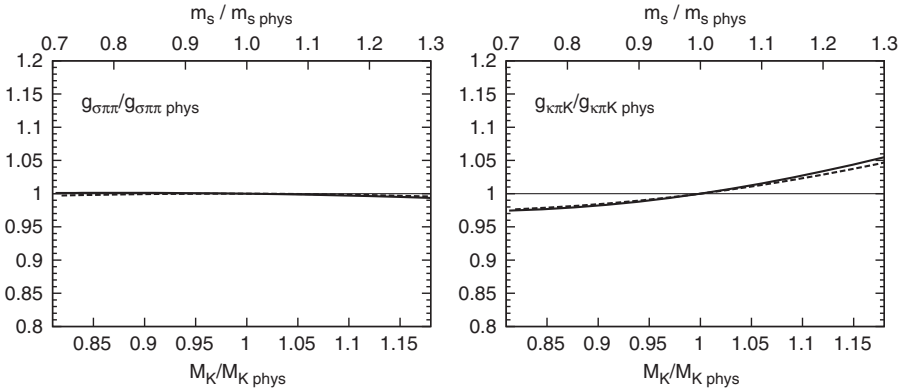

FIG. 13. Two-meson-scalar coupling dependence with respect to the strange quark mass m_s (horizontal upper scale), or the kaon mass (horizontal lower scale). Note we normalize the couplings to their physical values. We show on the left the $f_0(600)$ or sigma coupling to two pions and on the right that of the $\kappa(800)$ to πK.

A much bigger effect is seen for the $\kappa(800)$ in the right panels, whose mass changes by as much as 12% from its physical value within the range of study, whereas the width changes by as much as 20%. However, its mass dependence, despite being somewhat stronger than for its vector counterpart $K^*(892)$, is still softer than for the kaon itself. This is the reason why, as the $\kappa(800)$ becomes lighter its width increases, and vice versa.

In the lower panels we have also plotted the expected naive phase space reduction. This time, however, as the sigma properties barely depend on the strange quark mass, we only see a significant deviation from that naive behavior in the case of the $\kappa(800)$.

2. Coupling to two mesons

For all means and purposes, with respect to strange quark mass variations, the sigma coupling to two mesons turns out to be a constant within our approximation, as can be seen in the left panel of Fig. 13.

In contrast, the $g_{\kappa\pi K}$ coupling shows some dependence on the strange quark mass. Actually, it grows by 6% when the kaon mass is increased by 18% from its physical value.

V. SUMMARY AND CONCLUSIONS

In this work we have studied the quark mass dependence of the light vector and scalar resonances generated as poles of meson-meson scattering elastic amplitudes within unitarized one-loop chiral perturbation theory. This dependence is of interest to relate lattice results to hadronic observables, but also for anthropic and cosmological considerations. The use of an SU(3) formalism extends previous studies within SU(2), allowing us to study the behavior of strange resonances like the $\kappa(800)$ and $K^*(892)$, but also to study variations not only of the light u and d quark masses, but also of the strange quark mass.

After a brief introduction on how ChPT provides a model independent expansion of pion, kaon, and eta masses and decay constants, as well as their two-body interaction amplitudes, we have reviewed how this series can be used inside a dispersion theory formalism to construct the so-called inverse amplitude method amplitudes that satisfy elastic unitarity while respecting the ChPT expansion. It has been known for a long time that the elastic IAM reproduces well the meson-meson elastic scattering data up to 800–1000 MeV, including the resonance region. Note that we have refrained for the moment to use the very successful coupled channel IAM precisely because at present it lacks a dispersive derivation, and we want to avoid as much model dependence as possible. Of course the experimental data may fix rather well the energy dependence but not so well the mass dependence. For that reason we have presented here a new IAM analysis including simultaneously the existing lattice results on meson masses, decay constants, and scattering lengths. We obtain a fairly good description of experiment and lattice data using chiral parameters rather similar to existing one- and two-loop determinations. No fine-tuning of parameters is required. Once this is done, we have varied the quark masses within certain ranges that ensure the applicability of the elastic IAM for the resonances under study: $\hat{m}/\hat{m}_{\rm phys} \leq 9$ and $0.7 < m_s/m_{s\,\rm phys} < 1.3$ ($\hat{m}$ is the average mass of the u and d quarks). In practice, in ChPT we have changed the squared pion and kaon masses, which, at leading order, are proportional to quark masses. Although we have shown in Fig. 1 that this simple approximation works within roughly 10% accuracy, we have carefully included the full one-loop corrections, and shown the quark and meson mass variation independently in all plots.

In the second Riemann sheet of these amplitudes, the IAM generates the—conjugated pairs of—poles associated to the vector $\rho(770)$, $K^*(892)$ and scalar $f_0(600)$ and $\kappa(800)$ resonances. Light vector resonances are well established and there is little relevance on whether we refer to their "pole" or Breit-Wigner mass and widths. In contrast, the scalar $f_0(600)$, or sigma and the $\kappa(800)$ are rather controversial due to their large apparent width and the lack of a Breit-Wigner shape in the meson-meson scattering phase shifts. To avoid complications, we have always

presented our results in terms of pole definitions of masses, widths, and couplings.

For the $f_0(600)$ and $\rho(770)$ resonances, which appear in $\pi\pi$ scattering, we have nicely confirmed the similar unitarized one-loop SU(2) ChPT analysis performed in [3]. When increasing $\hat{m}$ both the sigma and ρ masses grow faster than the pion mass, whereas their widths decrease. However, the $\rho(770)$ mass behaves smoothly in the whole quark mass range, whereas, roughly at $M_\pi \sim 340$ MeV, the $f_0(600)$ pole and its conjugated pair meet in the second Riemann sheet below threshold, producing a nonanalyticity—or apparent splitting in two branches—of the sigma mass in terms of M_π. In addition, we confirm that the $\rho(770)$ width decrease, as $\hat{m}$ grows, follows remarkably well the simple expectations of phase space reduction already found within the SU(2) formalism. Once again, such a simple behavior is not observed for the sigma.

Of course, the SU(3) formalism allows us now to study also the $K^*(892)$ and $\kappa(800)$ resonances in πK scattering. We find that both the mass and width of the $K^*(892)$ behave qualitatively and quantitatively in a very similar way to those of the $\rho(770)$, which could be expected given the fact that they belong to the same octet. In addition, we have explicitly calculated here their couplings to two mesons, from the residue of the partial wave at their associated pole, finding that they are both remarkably independent of the nonstrange quark mass, as suggested from the width behavior. The $K^*(892)$ coupling is quite well approximated by a constant, although not so well as in the ρ case. This could be of relevance when computing its width on the lattice as it has already been done for the ρ [23].

It therefore seems that light quark masses play no significant role in the *dynamics* of the dominant decay modes of vector mesons, namely $\rho \to \pi\pi$ and $K^* \to \pi K$, since their couplings seem to be independent of light quark masses and all their width variation can be attributed to the phase space modification due to changes in the masses of all particles.

Furthermore, this provides a hint, checked here by explicit calculation, that the KSRF relation, that approximates these couplings by $g \simeq M_V/2\sqrt{2}f_\pi$, holds to less than 5% when changing $\hat{m}$ from 0 to 9 times its physical value. It is remarkable that this relation is so well satisfied, first, because ours is a one-loop calculation, which, in principle includes higher order pion mass corrections to KSRF, and the pion mass becomes rather large, but, second, because our resonance masses come from unitarized amplitudes whereas f_π stems from the nonunitarized ChPT truncated series.

Concerning the $\kappa(800)$, its behavior is qualitatively similar to that of the sigma, including the apparent mass splitting in two branches, which is a feature that can only occur for scalars. However, the $\kappa(800)$ nonstrange quark mass dependence is softer than for the sigma. Still the pion mass where the $\kappa(800)$ apparent mass splitting occurs is similar to that of the sigma, although with bigger uncertainties $M_\pi \sim 340$–400 MeV. Of course, contrary to the vector case, one could now expect some differences between the two scalars since they do not necessarily belong to the same octet and actually, the sigma is believed to be predominantly the singlet state [27,28], and it could even allow for a glueball component. As we did with the vectors, in this work we have also calculated explicitly the behavior of the scalar couplings to two mesons under quark mass variations. We find a qualitatively similar behavior for both $g_{\sigma\pi\pi}$ and $g_{\kappa\pi K}$: contrary to vectors, they cannot be considered constant within the variation range, particularly when M_π comes close to the apparent mass splitting value, where it suffers a dramatic enhancement.

Finally, since we use the SU(3) formalism, we have been able to study the dependence of light resonance properties on the strange quark mass. Because of the fact that the physical mass of the kaons is already quite high but also because we want the $M_K + M_\eta$ threshold to be significantly above the $K^*(892)$ mass, we have limited our study to the range $0.7 < m_s/m_{s\,\mathrm{phys}} < 1.3$. As could be naively expected, and in contrast to strange resonances, the masses and widths of both the nonstrange ρ and σ are remarkably independent of the strange quark mass. This time, the $\kappa(800)$ mass has a much stronger dependence than that of the $K^*(892)$—actually, it grows a factor of 3 faster. Once again, the $K^*(892)$ width follows remarkably well the behavior dictated by phase space only, and we have checked that its πK coupling is almost independent of m_s. The KSRF relation is also a fairly good approximation in the whole energy range, although not as good as in the case of the nonstrange quark. Concerning the $\kappa(800)$, once again its coupling is strongly dependent on the quark mass, so that its width does not follow the naive phase space behavior.

In summary, we have presented an exhaustive study on the strange and nonstrange quark mass dependence of light scalar and vector resonances appearing in elastic Goldstone bosons scattering. For the future, this work could be extended to other light scalar mesons like the $f_0(980)$ and $a_0(980)$ using a coupled channel formalism, that is somewhat less rigorous as it has no dispersive derivation, and also is much more complicated due to the presence of the $K\bar{K}$ threshold.

To conclude, and apart from the interest for studies of constraints on hadronic properties from cosmological or anthropic considerations, we think that the quark mass dependence studied here will be within the reach of lattice studies in the not too distant future—it is already so for the ρ meson—and we expect our results to be useful in the chiral extrapolation of lattice results to physical values.

ACKNOWLEDGMENTS

We thank C. Hanhart, E. Oset, and G. Ríos for useful discussions, J. A. Oller for suggesting us to include the

KSRF relation in our study, and W. Dunwoodie for providing us with lists of experimental $K\pi$ data. This work was partially supported by the Spanish Ministerio de Educación y Ciencia research Contracts No. FPA2007-29115-E, No. FPA2008-00592, and No. FIS2006-03438, U. Complutense/Banco Santander Grants No. PR34/07-15875-BSCH and No. UCM-BSCH GR58/08 910309. We acknowledge the support of the European Community-Research Infrastructure Integrating Activity Study of Strongly Interacting Matter (acronym HadronPhysics2, Grant Agreement No. 227431) under the Seventh Framework Programme of EU.

[1] S. Aoki *et al.*, Phys. Rev. D **60**, 114508 (1999).
[2] K. F. Liu, Prog. Theor. Phys. Suppl. **168**, 160 (2007); C. McNeile and C. Michael, Phys. Rev. D **74**, 014508 (2006); M. G. Alford and R. L. Jaffe, Nucl. Phys. **B578**, 367 (2000); T. Kunihiro *et al.*, Phys. Rev. D **70**, 034504 (2004).
[3] C. Hanhart, J. R. Pelaez, and G. Rios, Phys. Rev. Lett. **100**, 152001 (2008).
[4] J. Nagata, S. Muroya, and A. Nakamura, Phys. Rev. C **80**, 045203 (2009); S. Prelovsek and D. Mohler, Phys. Rev. D **79**, 014503 (2009).
[5] C. J. Hogan, Rev. Mod. Phys. **72**, 1149 (2000); H. Oberhummer *et al.*, Science **289**, 88 (2000); T. Damour and J. F. Donoghue, Phys. Rev. D **78**, 014014 (2008); T. E. Jeltema and M. Sher, Phys. Rev. D **61**, 017301 (1999).
[6] J. K. Webb *et al.*, Phys. Rev. Lett. **82**, 884 (1999); V. V. Flambaum and E. V. Shuryak, Phys. Rev. D **67**, 083507 (2003); **65**, 103503 (2002).
[7] J. Gasser and H. Leutwyler, Nucl. Phys. **B250**, 465 (1985).
[8] G. Amoros, J. Bijnens, and P. Talavera, Nucl. Phys. **B602**, 87 (2001).
[9] P. Buettiker, S. Descotes-Genon, and B. Moussallam, Eur. Phys. J. C **33**, 409 (2004); S. Descotes-Genon and B. Moussallam, Eur. Phys. J. C **48**, 553 (2006).
[10] J. R. Pelaez, Mod. Phys. Lett. A **19**, 2879 (2004).
[11] V. Bernard, N. Kaiser, and U. G. Meissner, Phys. Rev. D **43**, R2757 (1991); Nucl. Phys. **B357**, 129 (1991); Phys. Rev. D **44**, 3698 (1991).
[12] A. Gomez Nicola and J. R. Pelaez, Phys. Rev. D **65**, 054009 (2002).
[13] T. N. Truong, Phys. Rev. Lett. **61**, 2526 (1988); **67**, 2260 (1991); A. Dobado *et al.*, Phys. Lett. B **235**, 134 (1990).
[14] A. Dobado and J. R. Peláez, Phys. Rev. D **47**, 4883 (1993); **56**, 3057 (1997).
[15] J. A. Oller and E. Oset, Nucl. Phys. **A620**, 438 (1997); **652**, 407(E) (1999).
[16] J. A. Oller, E. Oset, and J. R. Pelaez, Phys. Rev. Lett. **80**, 3452 (1998); Phys. Rev. D **59**, 074001 (1999); **62**, 114017 (2000); F. Guerrero and J. A. Oller, Nucl. Phys. **B537**, 459 (1999); **B602**, 641(E) (2001).
[17] A. Gomez Nicola, J. R. Pelaez, and G. Rios, Phys. Rev. D **77**, 056006 (2008).
[18] S. D. Protopopescu *et al.*, Phys. Rev. D **7**, 1279 (1973); P. Estabrooks and A. D. Martin, Nucl. Phys. **B79**, 301 (1974); G. Grayer *et al.*, Nucl. Phys. **B75**, 189 (1974); C. D. Froggatt and J. L. Petersen, Nucl. Phys. **B129**, 89 (1977); W. Hoogland *et al.*, Nucl. Phys. **B126**, 109 (1977); M. J. Losty *et al.*, Nucl. Phys. **B69**, 185 (1974); N. B. Durusoy *et al.*, Phys. Lett. **45B**, 517 (1973); P. Estabrooks, R. K. Carnegie, A. D. Martin, W. M. Dunwoodie, T. A. Lasinski, and D. W. G. Leith, Nucl. Phys. **B133**, 490 (1978); D. Aston *et al.*, Nucl. Phys. **B296**, 493 (1988); D. Linglin *et al.*, Nucl. Phys. **B57**, 64 (1973); L. Rosselet *et al.*, Phys. Rev. D **15**, 574 (1977); S. Pislak *et al.* (BNL-E865 Collaboration), Phys. Rev. Lett. **87**, 221801 (2001); P. Truoel, arXiv:hep-ex/0012012.
[19] S. R. Beane *et al.* (NPLQCD Collaboration), Phys. Rev. D **77**, 094507 (2008); **77**, 014505 (2008); **74**, 114503 (2006); Ph. Boucaud *et al.* (ETM Collaboration), Comput. Phys. Commun. **179**, 695 (2008).
[20] R. Kaminski, J. R. Pelaez, and F. J. Yndurain, Phys. Rev. D **77**, 054015 (2008).
[21] P. C. Bruns and U.-G. Meißner, Eur. Phys. J. C **40**, 97 (2005).
[22] P. Gerber and H. Leutwyler, Nucl. Phys. **B321**, 387 (1989); A. Nyffeler, Z. Phys. C **60**, 159 (1993); A. Dobado and J. R. Pelaez, Phys. Rev. D **59**, 034004 (1998).
[23] S. Aoki *et al.* (CP-PACS Collaboration), Phys. Rev. D **76**, 094506 (2007).
[24] K. Kawarabayashi and M. Suzuki, Phys. Rev. Lett. **16**, 255 (1966); Riazuddin and Fayyazuddin, Phys. Rev. **147**, 1071 (1966).
[25] I. Caprini, G. Colangelo, and H. Leutwyler, Phys. Rev. Lett. **96**, 132001 (2006); F. J. Yndurain, R. Garcia-Martin, and J. R. Pelaez, Phys. Rev. D **76**, 074034 (2007); R. Kaminski, R. Garcia-Martin, P. Grynkiewicz, and J. R. Pelaez, Nucl. Phys. B, Proc. Suppl. **186**, 318 (2009).
[26] C. Amsler *et al.* (Particle Data Group), Phys. Lett. B **667**, 1 (2008).
[27] D. Black, A. H. Fariborz, F. Sannino, and J. Schechter, Phys. Rev. D **59**, 074026 (1999).
[28] J. A. Oller, Nucl. Phys. **A727**, 353 (2003).
[29] R. Kaminski, G. Mennessier, and S. Narison, Phys. Lett. B **680**, 148 (2009).
[30] S. Weinberg, Phys. Rev. **130**, 776 (1963); V. Baru, J. Haidenbauer, C. Hanhart, Yu. Kalashnikova, and A. E. Kudryavtsev, Phys. Lett. B **586**, 53 (2004).
[31] D. Gamermann, J. Nieves, E. Oset, and E. R. Arriola, Phys. Rev. D **81**, 014029 (2010).